J Solid State Electrochem (2006) 10: 538–546
DOI 10.1007/s10008-006-0127-x

ORIGINAL PAPER

G. Amow · S. J. Skinner

Recent developments in Ruddlesden–Popper nickelate systems for solid oxide fuel cell cathodes

Received: 10 January 2006 / Accepted: 22 January 2006 / Published online: 22 April 2006

Abstract Motivated by recent work on the Ruddlesden–Popper material, $La_2NiO_{4+\delta}$, which was shown to be a superior oxide-ion conductor than conventional solid-oxide fuel cell cathode perovskite materials, we undertook A- and B-site doping studies of the Ruddlesden–Popper nickelate series in an attempt to identify other candidates for cathode application. In this paper, we summarize our most significant results for the $La_2Ni_{1-x}Co_xO_{4+\delta}$ and $La_{2-y}Sm_yNiO_{4+\delta}$ systems and more recently, the higher-order Ruddlesden–Popper phases $La_{n+1}Ni_nO_{3n+1}$ (n=2 and 3), which show greater promise as cathode materials than the n=1 compositions.

Keywords Ruddlesden–Popper · Nickelates · Solid oxide fuel cells · Cathode · Oxide-ion diffusion

Introduction

Recent trends in solid-oxide fuel cell (SOFC) research have targeted the development of new materials for cell components for intermediate-temperature operation due to performance and longevity issues of cell components associated with high-temperature operation. In particular, the conventional cathode materials, $La_{1-x}Sr_xMnO_{3-\delta}$ (LSM) and $La_{1-x}Sr_xCo_{1-y}Fe_yO_{3-\delta}$ (LSCF), are known to suffer mechanical cracking (a result of thermal expansion mismatching) and unwanted formation of insulating phases when yttria-stabilized zirconia (YSZ) is used as the electrolyte for high temperature operation.

With the discovery of new electrolyte materials, which have superior ionic conductivities in the intermediate-temperature range such as lanthanum-strontium-magnesium gallates $La_{1-x}Sr_xMg_{1-y}Ga_yO_{3-\delta}$ (LSGM) and ceria-doped gadolinia $Ce_{1-x}Gd_xO_{2-\delta}$ (CGO), it becomes necessary to identify alternative materials suitable for cathode use. It is in this regard that the Ruddlesden–Popper class of materials, particularly the nickelate series ($La_{n+1}Ni_nO_{3n+1}$; n=1), have garnered significant attention in recent years as an alternative cathode material [1–3]. This is largely due to the relatively large oxide-ion conductivity observed coupled with reasonable electrical conductivity. $La_2NiO_{4+\delta}$ exhibits a broad metal-insulating transition from ~500 to 600 K with a maximum electrical conductivity of ~100 S/cm [4, 5], which is quite reasonable for cathode use. The oxide-ion conductivity, which is at least an order of magnitude larger than the conventional perovskites in the intermediate-temperature range, is a consequence of excess oxygen ions that can be accommodated in the Ruddlesden–Popper structure. The Ruddlesden–Popper structure is comprised of alternating perovskite blocks with a rock-salt intergrowth; as n is increased, the number of perovskite blocks increases as shown in Fig. 1. The relatively open structural framework afforded by the rock-salt intergrowth allows for the accommodation of hyperstoichiometric oxide-ions in the rock-salt layer as interstitials. Indeed, a wide range of oxygen hyperstoichiometry δ was observed for the parent nickelate, $La_2NiO_{4+\delta}$ ($0 \le \delta \le 0.25$) [6–8]. The degree of hyperstoichiometry, which can have a profound effect on the structural and physical properties, is influenced by synthesis conditions. Also, several studies have shown that the hyperstoichiometry can also be influenced by varying the identity of the rare-earth or transition-metal cations. In particular, δ was observed to increase with the substitution of the larger lanthanum ion with the progressively smaller praseodymium and neodymium ions [9, 10], an observation that is also seen

G. Amow (✉)
Defence Research and Development Canada-Atlantic,
H/AVRS, 101 Colonel By Drive,
Ottawa, Ontario, K1A 0K2, Canada
e-mail: Gisele.Amow@drdc-rddc.gc.ca
Tel.: +1-613-9912615
Fax: +1-613-9912384

S. J. Skinner
Department of Materials,
Imperial College London,
Prince Consort Road,
London, SW7 2BP, UK

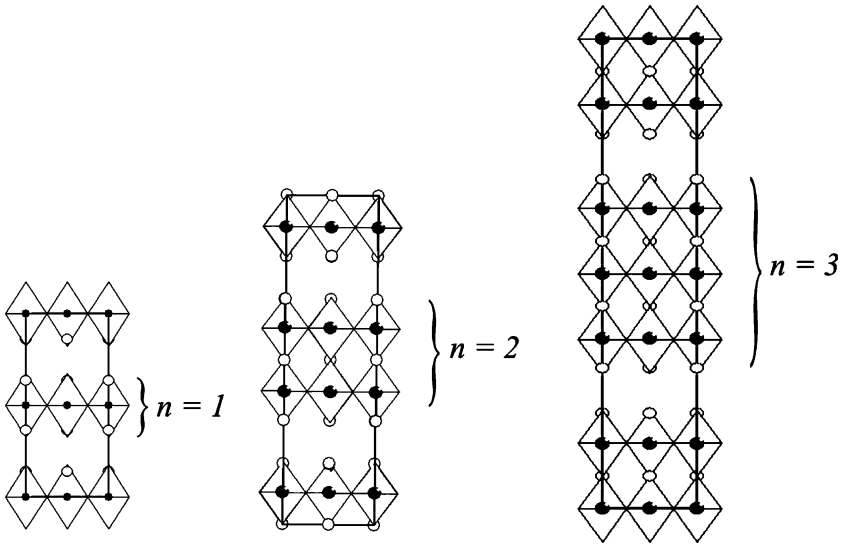

Fig. 1 Illustration of Ruddlesden-Popper structure ($La_{n+1}Ni_nO_{3n+1}$; n=1, 2, and 3)

with successive B-site doping with higher-valence ions such as iron and cobalt [11–14].

Despite these promising mixed-ionic electronic conducting characteristics, however, these materials have demonstrated poor electrode performance compared to LSM and LSCF and much work was undertaken to identify and optimize novel stoichiometries for improved performance. Consequently, we present in this paper a review of our previous work on Ruddlesden–Popper materials, which includes A-site and B-site doping studies of the n=1 series $La_2Ni_{1-x}Co_xO_{4+\delta}$ and $La_{2-y}Sm_yNiO_{4+\delta}$ and more recently, work on the higher-order n=2 and 3 Ruddlesden–Popper phases $La_3Ni_2O_{7-\delta}$ and $La_4Ni_3O_{10-\delta}$, which appear to be more promising as intermediate-temperature SOFC (ITSOFC) cathodes than the n=1 series of nickelates.

Materials and methods

Members of the $La_2Ni_{1-x}Co_xO_{4+\delta}$, $La_{2-y}Sm_yNiO_{4+\delta}$, and $La_{n+1}Ni_nO_{3n+1}$ (n=2 and 3) were prepared by the Pechini method [15]. In this technique, nitrate salts of the metal ions were dissolved in water to which a 1:1 molar ratio of ethylene glycol and citric acid was added. The molar ratios of ethylene glycol and citric acid to the nitrate salts were 4:1 in the case of the $La_2Ni_{1-x}Co_xO_{4+\delta}$ and $La_{2-y}Sm_yNiO_{4+\delta}$ solid solutions and 9:1 for $La_{n+1}Ni_nO_{3n+1}$ (n=2 and 3). The solutions were stirred and heated until majority of the water evaporated to leave behind a gel, which was further dried overnight under vacuum at ~453 K. The resulting foam-like residues after drying overnight were ground and prefired at 1,023 K for 4 h in air to remove unwanted organic residues. Pellets of 25-mm diameter of each composition were made from the treated powder and single-phase materials were obtained by firing under various temperatures.

Phase-purity and cell parameter determination was accomplished with a Bruker D8 X-ray powder diffractometer. For these purposes, data were collected with CuKá radiation for $10° \leq 2\theta \leq 100°$ with a step-size of 0.02° and t=10 s.

For oxygen content determination, standard iodometric titration via potentiometric methods was employed with a MetrOhm 751 GDP Titrino autotitrator. In addition, to substantiate these results, thermogravimetric analysis under the reducing conditions of 5% H_2-Argon was carried out. Nominal cation contents were assumed in the calculations for both techniques.

High-temperature electrical conductivity measurements were performed by the four-probe van der Pauw technique with a home-built instrument controlled by Labview software. Typical sample sizes were ~1 cm^2 with a thickness of ~1.8 mm with >85% theoretical density for the $La_2Ni_{1-x}Co_xO_{4+\delta}$ and $La_{2-y}Sm_yNiO_{4+\delta}$ systems. For the $La_{n+1}Ni_nO_{3n+1}$ (n=2 and 3) compositions, only ~54% theoretical density was obtained despite isostatic cold pressing at 300 MPa. Data were collected from T=RT to ~1,123 K in static air.

A two-probe AC impedance method was employed to determine the electrode performances of these materials in symmetrical cells with either $La_{1-x}Sr_xGa_{0.80}Mg_{0.20}O_{3-\delta}$ (x=0.1 or 0.2) or $Ce_{0.90}Gd_{0.10}O_{2-\delta}$ (CGO-10) as the electrolyte. The LSGM and CGO pellets were prepared by firing at 1,450°C for 6 h to achieve >95% theoretical density. AC impedance spectra were recorded with a 1260 Solatron frequency response analyzer, performing temperature hysteresis measurements over the frequency range of 15 Mhz to 0.01 Hz from 723 to 1,123 K in static air. A signal amplitude of 50 mV was applied. The symmetrical cells were prepared either by brush-coating or spraying ink of the doped-nickelates onto the dense LSGM or CGO

electrolytes. To promote adhesion, the coated pellets were subsequently fired at 900 °C for 4 h in air.

Oxide-ion diffusion and surface exchange data on the nickel-cobalt series were collected using a well-established isotopic exchange/secondary ion mass spectrometry (SIMS) analysis technique [16]. Each of the materials to be investigated were sintered into dense bodies of greater than 95% of theoretical density and subsequently polished using a combination of SiC paper and diamond polishing media to achieve a finish of 0.25 μm, giving a flat surface on which SIMS analysis could be performed. Each sample was then annealed in research grade $^{16}O_2$ before being exchange annealed in $^{18}O_2$. The details of the exchange procedure and exact conditions used are given elsewhere [17]. After annealing and quenching, each sample was cross-sectioned and polished to enable SIMS line scans to be undertaken using an Atomika 6500 instrument. From these data, oxygen diffusion and surface exchange coefficients were extracted through fitting of the data to Fick's second law of diffusion for a semi-infinite medium as discussed elsewhere [18, 19].

Results and discussion

The $La_2Ni_{1-x}Co_xO_{4+\delta}$ system

The B-site cobalt-doped system is of interest due to the possible improvement of the catalytic properties for the oxygen reduction process at the cathode as a consequence of cobalt being present. This system was previously investigated, however, only a few compositions were prepared successfully as single phases, $0.0 \le x \le 0.20$ [20]. In our work, the entire solid-solution series, $0.0 \le x \le 1.0$ was prepared for the first time, which afforded detailed investigations into the evolution of the structural and physical properties and hyperstoichiometry δ as cobalt is introduced [13, 21].

X-ray diffraction and oxygen content

The prepared compositions $0.0 \le x \le 1.00$ ($\Delta x = 0.10$) were obtained as black powders by the Pechini method. Due to stability issues, the $0.0 \le x \le 0.20$ compositions were prepared in air, while for the remaining compositions $0.30 \le x \le 1.00$, a reducing atmosphere of argon was required to obtain single-phase materials. Hyperstoichiometry δ was observed in all compositions as determined by iodometric titration and thermogravimetric analysis under reducing conditions with an apparent trend of increased δ with increased cobalt content x as shown in Fig. 2. For the air-prepared compositions, $0.0 \le x < 0.30$, δ increases systematically until $x \ge 0.30$ where a drastic decrease in δ is observed in accordance with the decreased oxygen partial pressure present when synthesized under flowing argon. An investigation by neutron powder diffraction revealed a structural phase transformation to occur within the series

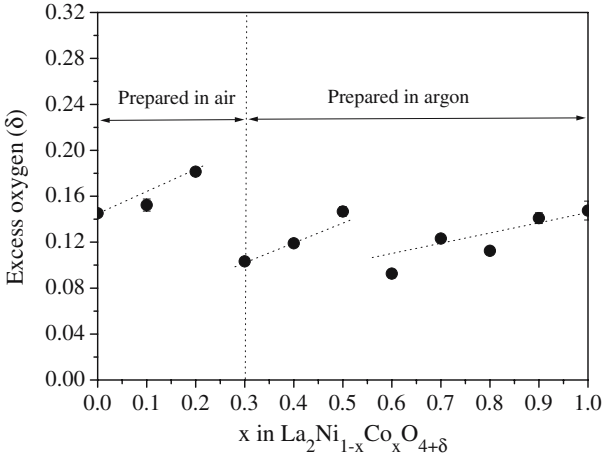

Fig. 2 Hyperstoichiometric oxygen δ vs cobalt-content (x) in $La_2Ni_{1-x}Co_xNiO_{4+\delta}$

with *F4/mmm* tetragonal symmetry observed for $0.0 \le x \le 0.5$ and *Bmab* orthorhombic symmetry for $0.6 \le x \le 1.0$.

Electrical conductivity

The temperature dependence of the electrical conductivity for the $La_2Ni_{1-x}Co_xO_{4+\delta}$ series is shown in Fig. 3. The broad metal-insulating transition at ~600 K observed for the parent nickelate, $La_2NiO_{4+\delta}$, is in reasonably good agreement with previous studies. However, as cobalt is successively introduced, the system tends toward insulating behavior until x~0.7. Furthermore, as more cobalt is introduced for x>0.7, the conductivity is observed to increase slightly until x=1.0. To understand these trends, structural and geometrical bond information was obtained by neutron diffraction. Recall, the electronic conductivity of Ruddlesden–Popper materials is dominated by the

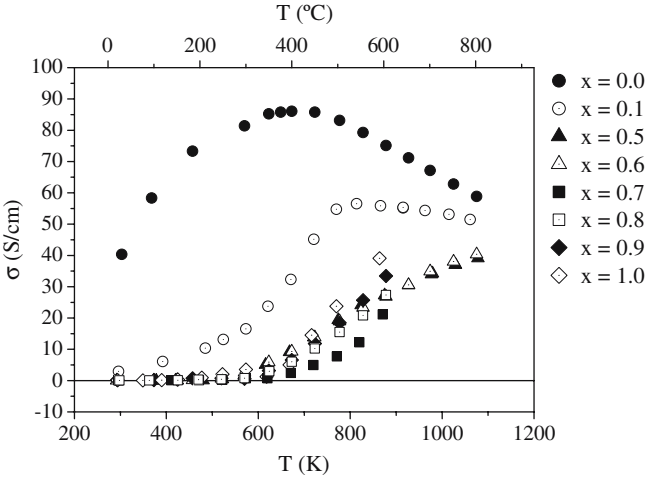

Fig. 3 Electrical conductivity vs T for $La_2Ni_{1-x}Co_xNiO_{4+\delta}$ system in air

transition-metal-oxygen-transition-metal interactions in the basal plane of the perovskite layer. Thus, in the $La_2Ni_{1-x}Co_xO_{4+\delta}$ system, this progressive insulating behavior in the tetragonal phases from x=0.1 to ~0.7 as more cobalt is introduced is consistent with the increased Ni(Co)–O1 bond length observed; longer bond lengths imply a decrease of the Ni(Co)–O covalent interactions, which leads to a decrease in the electronic conductivity. For x>0.7, the increased conductivity is attributed to the deviation of Ni(Co)–O–Ni(Co) bond angle from 180° in tetragonal to orthorhombic symmetry observed in these phases from the neutron diffraction data.

Electrode performance

Comparative studies of the electrode performance of selected compositions of the $La_2Ni_{1-x}Co_xO_{4+\delta}$ series were carried out with CGO-10 and LSGM-9182 because these electrolyte materials possess relatively similar oxide-ion conductivities over the intermediate-temperature range. They also possess comparable thermal expansion coefficients (TEC) of ~13.4×10^{-6} and 12×10^{-6} K^{-1} (CGO-10 and LSGM-9182, respectively) [22, 23], when compared to the TEC of $La_2NiO_{4+\delta}$ at ~13.7×10^{-6} K^{-1} [2]. Specifically, the LSGM-9182 and CGO-10 pellets were coated with cathode inks of x=0.0, 0.1, 0.3, and 0.5 and fired at 1,273 K for 2 h in argon. It was determined early on that the electrode performance on LSGM was consistently better than CGO; for example, see Fig. 4.

Given the superior area-specific resistance (ASR) values obtained with LSGM, we compare the normalized ASR values for the x=0.0, 0.1, 0.3, and 0.5 phases on LSGM as shown in Fig. 5. The data shows that the poorest electrode performance (larger ASR values) was achieved with the x=0.3 phase with the x=0.0, 0.1, and 0.5 compositions having similar values. It should be noted that the divergence of the ASR values at higher temperatures for the x=0.0 phase may be related to the variation in the oxygen nonstoichiometry of these materials as a function of temperature.

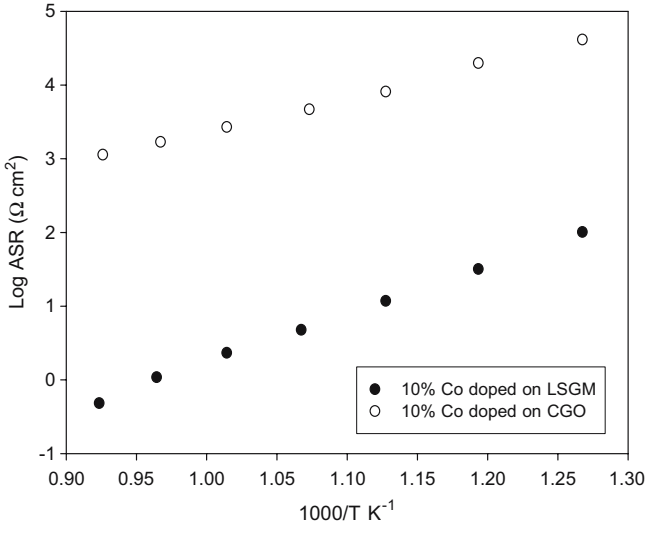

Fig. 4 Log ASR vs 1/T for $La_2Ni_{1-x}Co_xNiO_{4+\delta}$ (x=0.1) on CGO-10 and LSGM-9182 in air

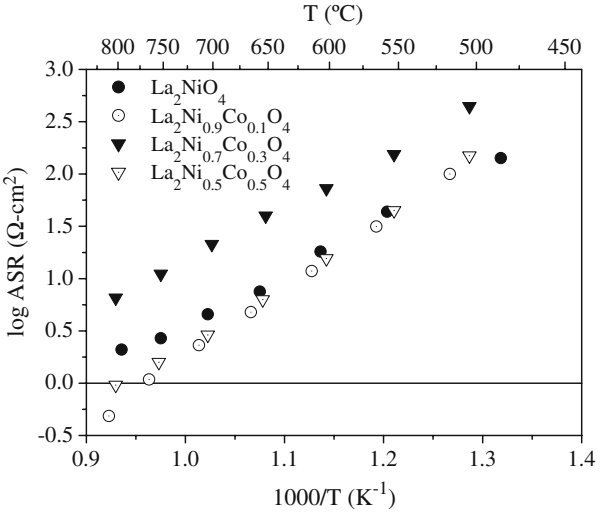

Fig. 5 Log ASR vs 1,000/T for $La_2Ni_{1-x}Co_xNiO_{4+\delta}$ (x=0.0, 0.1, 0.3, and 0.5) on LSGM-9182 in air

Oxide-ion diffusion measurements

Oxygen tracer diffusion measurements of the $La_2Ni_{1-x}Co_xO_{4+\delta}$ materials revealed two main features of the oxygen mobility within these materials [17]. Firstly, there is significant variation in the temperature dependence of the diffusivity of the materials with increasing Co content and secondly, that the normal linear temperature dependence of diffusion is not obeyed for the x=0.5 and 0.8 compositions. At low Co contents, there is a significant temperature dependence of the tracer diffusion coefficients leading to materials with activation energies of the order of 80–100 kJmol^{-1}, see Fig. 6. As the Co content increases, there

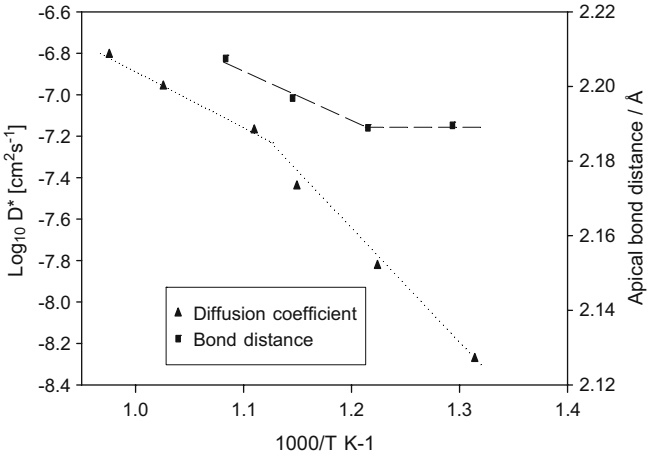

Fig. 6 Variation of diffusion coefficient and apical bond distance with temperature. Take note that the *lines* are a guide to the eyes only

is an apparent decrease in the activation energy of diffusion with the high cobalt content materials having a remarkably low activation energy of between 10 and 20 kJmol^{-1}. Due to these features, the nickel cobaltate materials are viewed as good candidates for relatively low temperature cathodes (773–873 K) assuming that material stability issues can be resolved. These data confirm the earlier studies of the diffusion process in the $La_2Ni_{1-x}Co_xO_{4+\delta}$ ($0 \le x \le 0.2$) [20, 24, 25] and show the good agreement obtained between independent studies of the lanthanum nickelates. The work that was undertaken on the Co-doped materials clearly shows an enhancement of the low temperature diffusion properties.

It is of further interest to consider the origin of the change in diffusion process at ~823 K in the x=0.5 and 0.8 Co-doped materials. The most likely reason for these changes is some structural transformation on heating and therefore in situ data from neutron powder diffraction studies was collected to confirm this. However, no discrete phase change could be identified and it is only on investigation of the bond lengths that some trends become apparent. The majority of the changes concern the apical transition-metal-oxygen bond length and on examination of the changes, it is obvious that a significant effect is observed at ~823 K (see Fig. 7). It is likely that these changes are associated with changes in the oxygen stoichiometry and further analysis of the neutron diffraction data should reveal the full complexity of this system.

Of further interest and evident from Fig. 7 is the superior performance of the Ni-Co based materials in terms of oxygen tracer diffusion at relatively low temperatures when compared to the conventional cathode materials. Currently, $La_{0.7}Sr_{0.3}CoO_{3-\delta}$ (LSC) is the best perovskite type oxide ion conductor and it is clear that the materials that we investigated are ~0.5 orders of magnitude lower than this material. However, it is well known that LSC has significant stability issues and therefore, the commonly used ITSOFC cathode material is the $La_{1-x}Sr_xCo_{1-y}Fe_yO_{3-\delta}$ composition. On comparing these new materials with LSCF, it can be seen that the low temperature oxide-ion diffusivity is several orders of magnitude higher for all of the K_2NiF_4 type oxides and therefore, based only on this criterion, would appear to be the more attractive cathode composition for ITSOFCs.

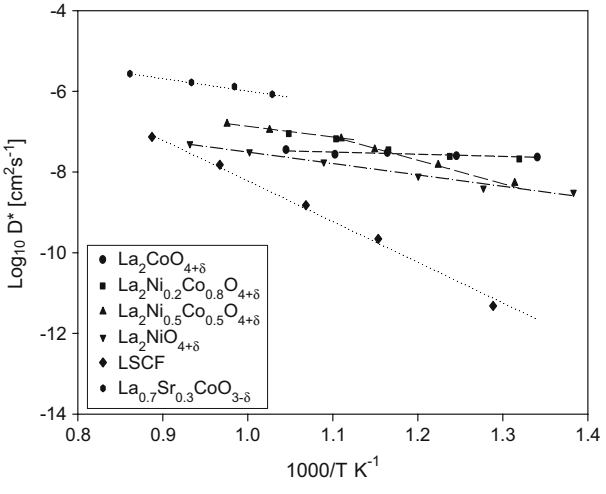

Fig. 7 Diffusion data of $La_2Ni_{1-x}Co_xO_{4+\delta}$ (x=0.0, 0.1, 0.3, and 0.5) compared with data for ABO_3 cathode materials. $La_{0.7}Sr_{0.3}CoO_{3-\delta}$ (LSC) data from [33], $La_{0.6}Sr_{0.4}Co_{.2}Fe_{0.8}O_{3-\delta}$ (LSCF) from [34], and $La_2NiO_{4+\delta}$ from [12]

The $La_{2-y}Sm_yNiO_{4+\delta}$ system

As mentioned in the introduction, a decrease in the lanthanide radii as one goes from $La_2NiO_{4+\delta}$ to $Nd_2NiO_{4+\delta}$ and $Pr_2NiO_{4+\delta}$ results in an increase in oxygen hyperstoichiometry δ with reported improvements of the electrode performance on YSZ. By extension, it would seem plausible that introduction of samarium would also have a favorable effect on increasing δ. However, given the relatively small ionic radii of samarium, $Sm_2NiO_{4+\delta}$ does not exist. Thus, the A-site samarium-doped solid solution was investigated to determine the effect of A-site doping by samarium on δ and its effects on structural and physical properties.

X-ray diffraction and oxygen content

Due to the relatively small ionic radii of samarium, $La_{2-y}Sm_yNiO_{4+\delta}$ was prepared as a truncated series with only single-phase materials obtained in the range $0.0 \le y \le 1.1$ (Δy=0.1) [13]. All compositions in this range were black and were identified as tetragonal *F4/mmm* by X-ray powder diffraction for all values of y studied with the cell volume decreasing linearly according to Vegard's law. It is interesting to note that although the prepared compositions were hyperstoichiometric, a clear dependence of the observed hyperstoichiometry δ with samarium doping

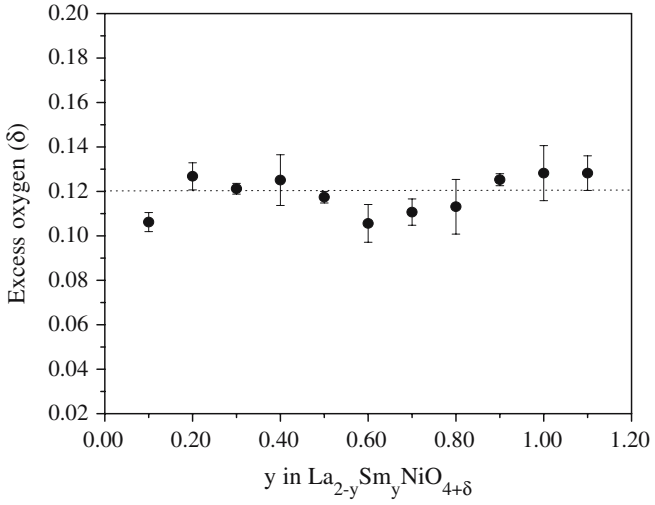

Fig. 8 Hyperstoichiometric oxygen δ vs samarium-content (y) in $La_{2-y}Sm_yNiO_{4+\delta}$

could not be found as was the case for the $La_2Ni_{1-x}Co_xO_{4+\delta}$ system (see Fig. 8).

Electrical conductivity

The electrical conductivity for the $La_{2-y}Sm_yNiO_{4+\delta}$ series is shown in Fig. 9. Unlike the $La_2Ni_{1-x}Co_xO_{4+\delta}$ system, the broad maximum observed in the parent $La_2NiO_{4+\delta}$ is retained for all compositions. From the data, it is clear that samarium substitution causes an increase in the overall conductivity values. However, it is interesting to note, particularly for $y \leq 0.50$, that the electrical conductivity values vary nonsystematically with samarium content δ or unit-cell volume and may be due to subtle variances in the density of the pellets used for the measurements. Take note in Fig. 9 that there is an apparent broadening of the maximum conductivity regime as one goes from x=0.1 to 1.1, which is not yet well understood at this time and may be of practical use where enhanced electronic conductivity is required at elevated temperatures.

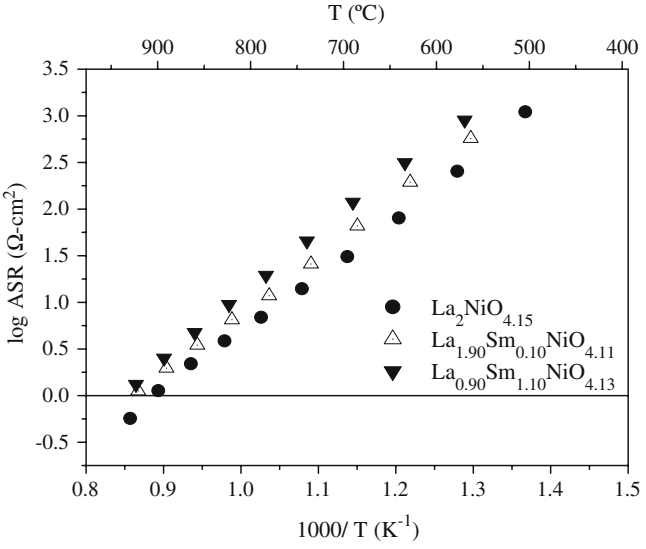

Fig. 10 Log ASR vs 1,000/T for $La_{2-y}Sm_yNiO_{4+\delta}$ (x=0.0, 0.1, and 1.1) on LSGM-8282 in air

Electrode performance

Based on the favorable ASR values obtained for the $La_2Ni_{1-x}Co_xO_{4+\delta}$ when LSGM is used instead of CGO, the electrode performance of the $La_{2-y}Sm_yNiO_{4+\delta}$ system was determined only for symmetrical cells made with LSGM-8282. To determine the range in the electrode performance of the series, inks of the end members x=0.0, 0.1 and 1.1 compositions were brush-coated onto LSGM-8282 pellets, which were subsequently fired at 1,173 K for 4 h in air. The normalized ASRs are shown in Fig. 10 where the lowest overall ASR values are found for the parent $La_2NiO_{4+\delta}$, and become progressively worse as x increases from 0.1 to 1.1. A discoloration on the surface of the x=1.1 coated pellet was observed after the measurement, which was revealed by X-ray powder diffraction to be a mixed Ni^{2+}/Ni^{3+} impurity phase. However, no similar degradation was observed for the x=0.1 phase.

The n=2 and 3 Ruddlesden–Popper nickelates: $La_3Ni_2O_{7-\delta}$ and $La_4Ni_3O_{10-\delta}$

In the studies of the n=1 cobalt- and samarium-doped systems, it was discovered that although certain gains were made in terms of the electrical conductivity as in the case of $La_{2-y}Sm_yNiO_{4+\delta}$ or electrode performance of such materials, e.g., $La_2Ni_{1-x}Co_xO_{4+\delta}$ (x=0.1 and 0.5), stability became a critical issue when considering their practical use as cathodes. In this regard, it was determined that the n=1 nickelate series fall short of being suitable candidates as thermal aging at 1,173 K for 2 weeks in air of the parent nickelate, $La_2NiO_{4+\delta}$, resulted in the formation of a mixed-valent impurity phase as shown in Fig. 11. This observation led to a recent investigation of the higher-order $La_3Ni_2O_{7-\delta}$

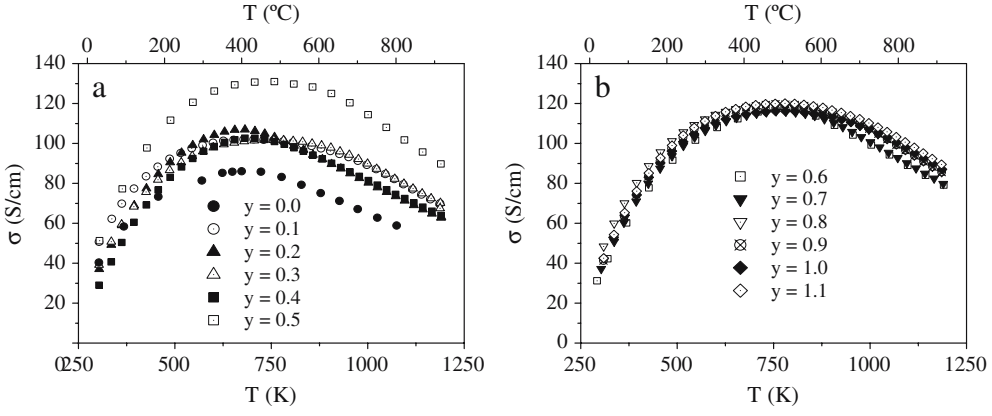

Fig. 9 Electrical conductivity vs T for $La_{2-y}Sm_yNiO_{4+\delta}$ system in air

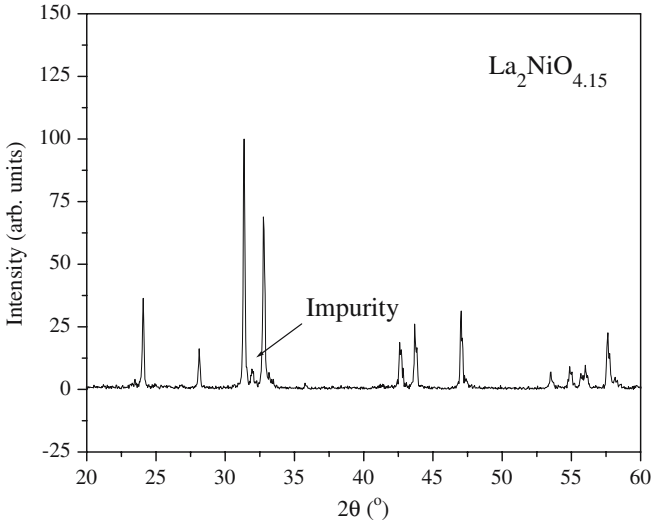

Fig. 11 Impurity phase formation of $La_2NiO_{4.15}$ after aging for 2 weeks at 1,173 K in air

and $La_4Ni_3O_{10-\delta}$ as potential SOFC cathodes given the presence of increased amounts of Ni^{3+} in these mixed-valent Ni^{2+}/Ni^{3+} oxides [26]; the Ni^{3+} ion is relatively more stable in air than Ni^{2+} below 1,173 K as evidenced by the stability of $LaNiO_3$ in air below this temperature. Consequently, these materials are expected to exhibit improved thermal stability compared to the predominantly Ni^{2+} n=1 nickelate series. Finally, these materials are made particularly even more attractive given their known metallic behavior at room temperature, which persists at higher temperatures as found for $La_4Ni_3O_{10-\delta}$ [27].

X-ray diffraction and oxygen content

The $La_3Ni_2O_{7-\delta}$ and $La_4Ni_3O_{10-\delta}$ compositions were prepared as black powders by the Pechini method and the X-ray powder diffraction patterns were indexed as orthorhombic *F*/*mmm*. Due to the difficulty of readily dissolving these two phases in acid for iodometric titration, thermogravimetric analysis under a reducing 5% H_2/Argon gas mixture was used for oxygen content determination. Unlike the $La_2Ni_{1-x}Co_xO_{4+\delta}$ and $La_{2-y}Sm_yNiO_{4+\delta}$ series of compounds, the n=2 and 3 phases are oxygen-deficient with δ=−0.05 and −0.22, respectively, in agreement with a previous study utilizing similar preparation techniques [28]. A study on the thermal stability of these compositions showed no impurity phase formation when aged at 1,173 K for 2 weeks in air when compared to $La_2NiO_{4+\delta}$ [26].

Electrical conductivity

The electrical conductivity of $La_2NiO_{4.15}$, $La_3Ni_2O_{6.95}$, and $La_4Ni_3O_{9.78}$ are shown in Fig. 12. When the relatively low theoretical densities of ~54% for the n=2 and 3 samples used for the measurement are taken into account, the electrical conductivities for these phases are likely to be significantly higher than $La_2NiO_{4.15}$ as shown. Reasonably, with the progressive increase in the number of perovskite layers from n=1 to 3, the electrical conductivity is expected to systematically increase due to the increasing number of Ni–O–Ni interactions in the perovskite layers, which are responsible for the electronic conduction pathways. Such a systematic trend with n is mirrored in the low temperature regime <300 K and borne out of the predicted electronic structures of these materials [29, 30]. It is also interesting to note the peculiar anomalies observed in the temperature-dependence of the electrical conductivity for $La_3Ni_2O_{6.95}$ and $La_4Ni_3O_{9.78}$ at ~548 K. As evidenced by preliminary X-ray diffraction measurements, which show a phase transition from orthorhombic to tetragonal symmetry for both compositions, these anomalies may be structural in origin [31]. This is also reflected in the thermal expansion measurements, which show a change in slope at ~548 K, most noticeably for $La_3Ni_2O_{6.95}$ (see Fig. 13). On this latter point, the measured thermal expansion coefficients α from 348 to 1,173 K were found to be 13.8×10^{-6} K^{-1} for $La_2NiO_{4.15}$, which is in agreement with previous literature values [2, 32], while α remains essentially the same at $\sim13.2\times10^{-6}$ K^{-1} for both $La_3Ni_2O_{6.95}$ and $La_4Ni_3O_{9.78}$ over the same temperature range.

Electrode performance

Symmetrical cells were prepared by brush-coating inks of $La_3Ni_2O_{6.95}$ and $La_2NiO_{4.15}$ onto dense LSGM-9182 pellets, which were then fired at 1,173 K in air for 4 h. The normalized area-specific resistance for symmetrical cells with LSGM-9182 is shown in Fig. 14. From this data, the $La_4Ni_3O_{9.78}$ coated pellet has the lowest ASR values with an activation energy of E_a=1.36 eV followed by $La_3Ni_2O_{6.95}$ and $La_2NiO_{4.15}$ with E_a=1.24 and 1.27 eV,

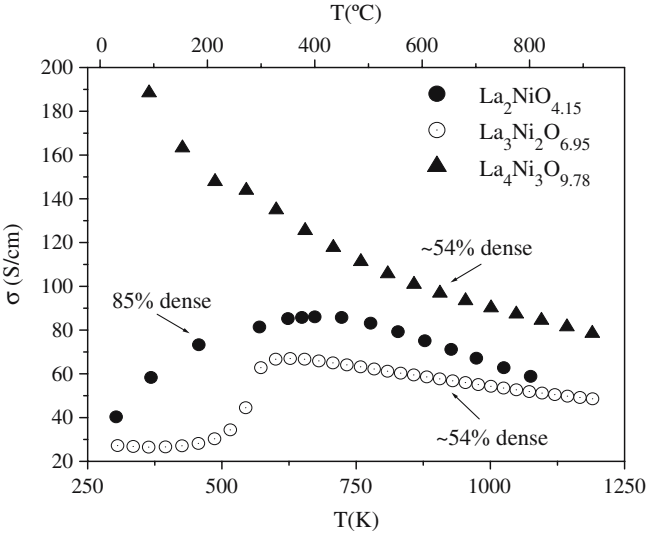

Fig. 12 Electrical conductivity vs T for $La_2NiO_{4.15}$, $La_3Ni_2O_{6.95}$, and $La_4Ni_3O_{9.78}$ in air

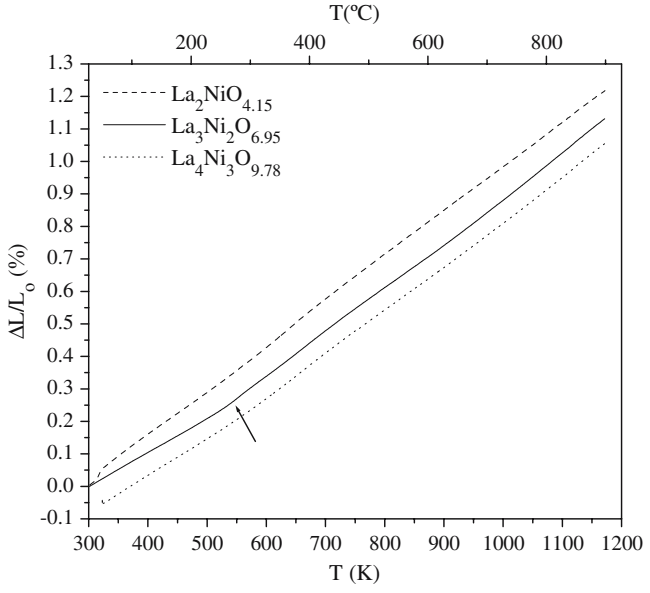

Fig. 13 Relative thermal expansion for $La_2NiO_{4.15}$, $La_3Ni_2O_{6.95}$, and $La_4Ni_3O_{9.78}$ in air

respectively. At first glance, it would appear that the observed trend might correlate with the electrical conductivity as *n* is increased. However, it is also very likely that the systematic oxygen deficiency with *n* may also play a vital role in facilitating improved oxide-ion conduction by providing vacant oxygen sites in the perovskite layers. This latter point requires further investigation with neutron diffraction studies to determine the distribution of oxide-ion vacancies and oxide-ion diffusion measurements for these phases.

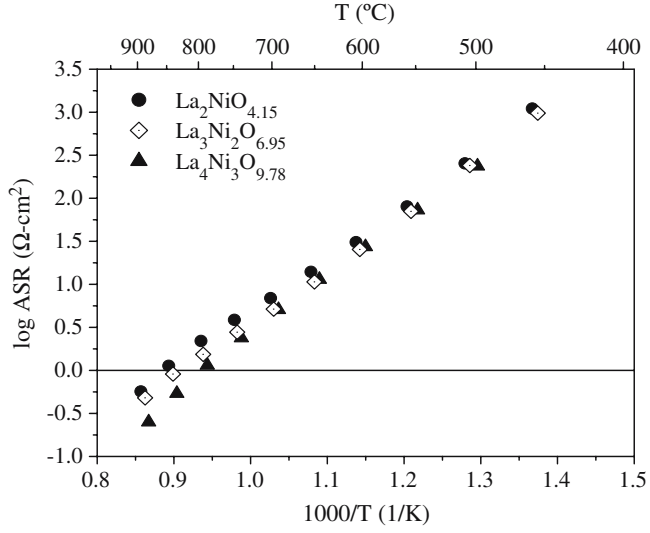

Fig. 14 Log ASR vs 1,000/T for $La_2NiO_{4.15}$, $La_3Ni_2O_{6.95}$, and $La_4Ni_3O_{9.78}$ on LSGM-9182 in air

Conclusions

This paper summarizes our work in the development of novel nickel-based materials for ITSOFC cathodes based on the Ruddlesden–Popper structure. Doping studies on the A- and B-sites were carried out with samarium and cobalt *n*=1 nickelate series, respectively, which has led to more recent investigations into the higher-order Ruddlesden–Popper phases, $La_3Ni_2O_{7-\delta}$ and $La_4Ni_3O_{10-\delta}$. From these investigations, several salient conclusions can be made. Invariably, all *n*=1 compositions studied were prepared as hyperstoichiometric phases. It was seen that cobalt doping on the B-site results in lowered electrical conductivities as more cobalt is introduced, whereas this property is improved with samarium doping on the A-site while retaining the temperature-dependence behavior as found for $La_2NiO_{4+\delta}$.

The electrode performance of the *n*=1 materials show consistently improved electrode performances when LSGM is used as an electrolyte compared to CGO. These differences may be due to lattice mismatches, which may arise from differences with the perovskite nature of LSGM and fluorite CGO, or may be due to possible reactions of CGO with nickel in these materials; further studies will be required to determine if these are valid scenarios.

Increasing the cobalt content in *n*=1 phases dramatically improves the low temperature oxide ion conductivity. Remarkably, low activation energies were found for the higher cobalt contents offering the possibility of low temperature cathode operation. However, the use of the *n*=1 nickelate Ruddlesden–Popper phases as cathodes is tentative because of their long-term stability at elevated temperatures as shown by the degradation of $La_2NiO_{4+\delta}$ when aged for 2 weeks in air at 1,173 K. As such, further investigations to improve the stability of the *n*=1 Ruddlesden–Popper nickelate phases are required.

Recently, investigations into the higher-order *n*=2 and 3 Ruddlesden Popper phases were performed. These phases were obtained as oxygen-deficient $La_3Ni_2O_{7-\delta}$ and $La_4Ni_3O_{10-\delta}$. Despite this, however, and relative to $La_2NiO_{4+\delta}$, these materials exhibit improved thermal stability, electrical conductivity, and electrode performance with comparable thermal expansion coefficients to LSGM. Consequently, $La_3Ni_2O_{7-\delta}$ and $La_4Ni_3O_{10-\delta}$ appear to be superior candidates for ITSOFC cathodes than $La_2NiO_{4+\delta}$ based materials and future investigations to characterize (such as oxide-ion diffusion measurements) and to optimize their performance for cathode operation are warranted.

Acknowledgements The authors thank the National Research Council Canada and the British Council for funding of the work on the $La_2Ni_{1-x}Co_xO_{4+\delta}$ and $La_{2-y}Sm_yNiO_{4+\delta}$ systems through the Joint Science and Technology program, grant reference 00CRP12.

References

1. Kharton VV, Viskup AP, Naumovich EN, Marques FMB (1999) J Mater Chem 9:2623
2. Skinner SJ, Kilner JA (2000) Solid State Ionics 135:709
3. Kharton VV, Yaremchenko AA, Tsipis EV, Frade JR (2003) Oxygen transport and electrochemical activity of La_2NiO_4-based cathode materials. In: Singhal SC, Dokiya M (eds) Proceedings of eighth international symposium on solid oxide fuel cells (SOFC-VIII), Paris, France, 2003, PV 2003-07. The Electrochemical Society, Pennington, NJ, pp 561–570
4. Ganguly P, Rao CNR (1973) Mater Res Bull 8:405
5. Bassat JM, Odier P, Loup JP (1994) J Solid State Chem 110:124
6. Jorgensen JD, Dabrowski B, Pei S, Richards DR, Hinks DG (1989) Phys Rev B 40:2187
7. Rodriguez-Carvajal J, Fernandez-Diaz MT, Martinez JL (1991) J Phys Condensed Matter 3:3215
8. Rice DE, Buttrey DJ (1993) J Solid State Chem 105:197
9. Bassat JM, Boehm E, Grenier JC, Mauvy F, Dordor P, Pouchard M (2002) In: Huijsmans J (ed) Fifth European solid oxide fuel cell forum, vol 2. Lucerne, Switzerland, p 586
10. Boehm E, Bassat JM, Dordor P, Mauvy F, Grenier JC, Stevens P (2005) Solid State Ionics 176:2717
11. Tichy RS, Huang KQ, Goodenough JB (2000) In: Wachsman ED, Weppner W, Traversa E, Vanysek P, Yamazoe N, Liu ML (eds) The Electrochemical Society proceedings, vol 2000-32. The Electrochemical Society, Phoenix, Arizona, p 171
12. Kilner JA, Shaw CKM (2002) Solid State Ionics 154–155:523
13. Amow G, Whitfield P, Davidson I, Munnings CN, Skinner SJ (2003) The Electrochemical Society proceedings, Orlando, USA (in press)
14. Yaremchenko AA, Kharton VV, Patrakeev MV, Frade JR (2003) J Mater Chem 13:1136
15. Pechini MP (1967) US Patent 3,330,697
16. Kilner JA (1996) In: Poulsen FW (ed) High temperature electrochemistry: ceramics and metals, proceedings of the Risoe international symposium on materials science. Risoe National Laboratory, Roskilde, Denmark
17. Munnings CN, Skinner SJ, Amow G, Whitfield PS, Davidson IJ (2005) Solid State Ionics 176:1895
18. Carter S, Selcuk A, Chater RJ, Kajda J, Kilner JA, Steele BCH (1992) Solid State Ionics 53–56:597
19. De Souza RA, Kilner JA (1998) Solid State Ionics 106:175
20. Shaw CKM, Kilner JA (2000) In: McEvoy J (ed) Fourth European solid oxide fuel cell forum, vol 2. Lucerne, Switzerland, p 611
21. Skinner SJ, Munnings CN, Amow G, Whitfield P, Davidson I (2003) In: Singhal SC, Dokiya M (eds) Proceedings of eighth international symposium on solid oxide fuel cells (SOFC-VIII), Paris, France, 2003, PV 2003-07. The Electrochemical Society, Pennington, NJ, p 552
22. Kharton VV, Figueiredo FM, Navarro L, Naumovich EN, Kovalevsky AV, Yaremchenko AA, Viskup AP, Carneiro A, Marques FMB, Frade JR (2001) J Mater Sci 36:1105
23. Stevenson JW, Hasinska K, Canfield NL, Armstrong TR (2000) J Electrochem Soc 147:3213
24. Bassat JM, Odier P, Villesuzanne A, Marin C, Pouchard M (2004) Solid State Ionics 167:341
25. Boehm E, Bassat JM, Mauvy F, Dordor P, Grenier JC, Pouchard M (2000) In: McEvoy J (ed) Fourth European solid oxide fuel cell forum, vol 2, Lucerne, Swizterland, p 717
26. Amow G, Davidson IJ (2005) In: Singhal SC, Misuzaki J (eds) SOFC-IX, vol 2005–007. Electrochemical Society, Quebec City, Quebec, Canada, p 1745
27. Vashuk VV, Olshevskaya, Savchenko VF, Puchkaeva EY (1994) Inorg Mater 30:1357
28. Carvalho MD, Cruz MM, Wattiaux A, Bassat JM, Costa FMA, Godinho M (2000) J Appl Phys 88:544
29. Zhang Z, Greenblatt M, Goodenough JB (1994) J Solid State Chem 108:402
30. Zhang Z, Greenblatt M (1995) J Solid State Chem 117:236
31. Amow G, Davdison IJ, Skinner SJ (2005) Solid State Ionics (in press)
32. Odier P, Nigara Y, Coutures J, Sayer M (1985) J Solid State Chem 56:32
33. van Doorn RE, Fullarton IC, de Souza RA, Kilner JA, Bouwmeester HJM, Burggraaf AJ (1997) Solid State Ionics 96:1
34. Lane JA, Benson SJ, Waller D, Kilner JA (1999) Solid State Ionics 121:201